J Nanostruct 16(3): 3914-3923, Summer 2026

RESEARCH PAPER

Evaluation of Silver Nanoparticles as In Vivo X-ray Contrast Agents: A Quantitative Image-Quality Comparison with Iodine in a Murine Tail-Vein Injection Model

Ameer Salim Khlaif [1], Mazin Kamil Hamid [1], Hadeel Mazin Kamil [2]*

[1] *Department of Physiology and Medical Physics, College of Medicine, Al-Nahrain University, Baghdad, Iraq*

[2] *Al- Karkh university of science, Baghdad, Iraq*

ARTICLE INFO

Article History:
Received 17 April 2026
Accepted 23 June 2026
Published 01 July 2026

Keywords:
Entropy
RMS contrast
Silver nanoparticle
Tail-vein injections
X-ray contrast agents

ABSTRACT

Iodine contrast vendors are still generic products used for contrast-enhanced X-ray computed tomography imaging however, silver nanoparticles (AgNPs) appealing due to the fact that their short circulation time, limited focused feasibility, and safety concerns in vulnerable patients have encouraged the development of alternative contrast agents. Silver nanoparticles (AgNPs) are attractive candidates because silver has a relatively high atomic number (Z = 47) and a K-edge energy of approximately 25.5 keV, which is relevant for low-energy diagnostic X-ray spectra and dual-energy imaging applications. This vision evaluated the in vivo X-ray contrast performance of intravenously administered AgNPs in mice and compared their quantitative photographic adequacy performance with an iodine-based fully saturated compound and a deionized water control. Healthy male mice with a mean body weight of approximately 20 g received a single 0.2 mL intravenous injection through the lateral tail vein. The injected materials were AgNP solutions at doses of 0.186, 0.25, 0.50, 0.75 mg/kg, and at 1.00 g/kg, iodine at 0.30 mg/kg, and deionized water. X-ray images were obtained at 1, 3, and 5 minutes after injection under fixed acquisition conditions. Quantitative image analysis was performed using consistent regions of interest. The evaluated metrics were mean intensity, root mean square (RMS) contrast, Michelson contrast, standard deviation, and entropy. The AgNPs 0.75 mg/kg group produced the strongest overall image-quality performance, especially at 3 minutes after injection. At this time point, it showed the highest mean intensity (84.56 arbitrary units) and the highest entropy (7.31), exceeding the corresponding iodine values. RMS contrast and Michelson contrast were useful supplementary measures, but they were interpreted cautiously because high values can also reflect noise, saturation, or heterogeneous nanoparticle distribution Intravenously administered AgNPs showed promising in vivo radiographic evaluation behavior in this murine version, with the most pronounced overall performance peak achieved at 0.75 mg/kg after 3 minutes. These effects guide further investigation of AgNPs as experimental X-ray evaluation providers.

How to cite this article
Khlaif A, Hamid M, Kamil H. Evaluation of Silver Nanoparticles as In Vivo X-ray Contrast Agents: A Quantitative Image-Quality Comparison with Iodine in a Murine Tail-Vein Injection Model. J Nanostruct, 2026; 16(3):3914-3923. DOI: 10.22052/JNS.2026.03.076

* *Corresponding Author Email: mazinkamil4@gmail.com*

INTRODUCTION

X-ray imaging remains one of the most widely used diagnostic tools in medicine. Iodinated contrast agents are routinely used to increase the visibility of blood vessels, organs, and lesions that would otherwise be difficult to distinguish on non-contrast images. Although iodine-based agents are clinically effective, they are small molecules that distribute nonspecifically and clear rapidly. Their use also requires careful consideration in patients with kidney disease or other risk factors. Current consensus guidance has clarified that the risk of contrast-associated acute kidney injury from modern intravenous iodinated agents has sometimes been overstated, but kidney safety remains an important clinical issue and should be described accurately rather than exaggerated [1]. Nanoparticle-based contrast agents are being investigated because they offer design flexibility that conventional small-molecule agents do not. A nanoparticle can carry a high payload of X-ray attenuating atoms, and its surface can be modified to alter circulation time, biological interactions, or tissue targeting. These features are especially relevant for dual-energy, spectral, and photon-counting imaging, where material-specific attenuation can be exploited [2,3]. Silver is a particularly interesting candidate for X-ray contrast research. It has an atomic number of 47 and a K-edge near 25.5 keV. Previous theoretical and experimental work has suggested that silver-based agents may provide useful contrast in dual-energy mammography and related low-energy X-ray systems [4,5]. Silica-encapsulated and PEGylated silver nanoparticles have also been investigated as dual-energy mammography contrast agents and have shown in vivo imaging potential in preclinical work [6]. The present study was designed to evaluate AgNPs as in vivo X-ray contrast agents in mice. The study compared several AgNPs dose levels with iodine and deionized water using quantitative image-quality metrics at three early post-injection time points. The purpose was not only to identify the brightest image, but also to compare image texture, dynamic range, and information content using a multi-metric approach. This matters because a single number can be misleading: high RMS contrast may indicate useful signal, but it may also reflect noise or nonuniform particle distribution. A stronger conclusion requires agreement across multiple measurements.

MATERIALS AND METHODS

Study design

This was an experimental in vivo X-ray imaging study conducted in a murine model. Male mice were assigned to receive AgNPs at one of five dose levels, an iodine-based contrast agent, or deionized water as a negative control. Each animal received a single intravenous tail-vein injection, followed by serial X-ray imaging at 1, 3, and 5 minutes after injection. Image quality was then quantified from digital images using predefined regions of interest. Healthy male mice with an average body weight of approximately 20 g were used. Animals examined before imaging to confirm that they are clinically healthy. They housed under controlled temperature, humidity, and light/dark cycle conditions with free access to food and water Animals monitored before injection, during imaging, and after recovery for signs of distress, abnormal respiration, impaired movement, tail injury, or injection-site leakage.

Preparation of AgNPs, iodine, and control solutions

AgNPs solutions were prepared at dose levels of 0.186, 0.25, 0.50, and 0.75 mg/kg, and at one high-dose level of 1.00 g/kg. The iodine comparator was prepared at 0.30 mg/kg. Deionized water was used as the negative control. All injected solutions were prepared freshly before administration using sterile technique. Solutions for intravenous injection was sterile, pyrogen-free when possible, and free of visible aggregates.

Nanoparticle characterization

The use of a number of complementary analytical strategies for AgNPs was widely characterized. The optical properties were detected using a Lambda 45 UV-Vis spectrophotometer in the wavelength range of 100–1000 nm. Surface charge and colloidal stability were assessed by zeta potential (ZP) analysis, which measures electrostatic repulsion between equally charged particles and presents a reliable indicator of nanosuspension body equilibrium [7,8]. Elemental composition was determined by energy-dispersive X-ray spectroscopy (EDS), which detects characteristic X-rays emitted from the sample upon electron beam exposure to identify and quantify the metal nanoparticles present on the sample surface [9]. Crystallographic structure, crystal size, and chemical composition were analyzed by X-ray diffraction (XRD), a non-destructive

technique that provides precise information on atomic arrangement and physical properties of nanomaterials [10,11]. Finally, particle morphology, size, homogeneity, and internal nanostructure were examined by scanning electron microscopy (SEM), which uses a focused electron beam to generate high-resolution images of the surface of the sample at the nanoscale [12-14].Together, these techniques provided a complete physicochemical profile of the AgNPs, with each method contributing complementary information as described in the Results section. because AgNPs biodistribution and toxicity depend strongly on particle size, surface chemistry, charge, coating, and aggregation behavior [15].

Tail- vein injection

Each mouse received 0.2 mL of the assigned solution by intravenous injection through the lateral tail vein. Before injection, the tail was gently warmed to dilate the vein, and the injection site should be cleaned with 70% alcohol. A sterile small-gauge needle, commonly 27-30 G was used. The needle should be inserted bevel-up into the lateral tail vein at a shallow angle. Correct placement is indicated by smooth injection without resistance, absence of swelling at the injection site, and blanching of the vein during administration. The solution injected slowly to reduce the risk of vascular injury, leakage, acute volume stress, or pulmonary/cardiac effects. During imaging, each mouse was positioned consistently to reduce variation in attenuation and region-of-interest placement.

X-ray imaging

X-ray images were acquired at 1, 3, and 5 minutes after injection. The same imaging system and acquisition parameters were used for all groups and time points. The device model, tube voltage (kVp) was 50, tube current- was 50 (mA), exposure time 0.2 second. A fixed imaging protocol was used to allow direct comparison among AgNP, iodine, and water groups. The DICOM images are available, calibrated intensity.

Region of interest and image analysis

Digital images were analyzed using consistent regions of interest. The present analysis included mean intensity, RMS contrast, Michelson contrast, and entropy. Mean intensity was defined as the average pixel value within the ROI. Standard deviation described the spread of pixel values around the mean. RMS contrast measured the root mean square variation of pixel intensities. Michelson contrast was calculated as (Imax - Imin) / (Imax + Imin), where Imax and Imin are the maximum and minimum pixel values in the ROI. Entropy was calculated from the gray-level probability distribution and used as an estimate of image information content. All metrics should be interpreted together rather than in isolation.

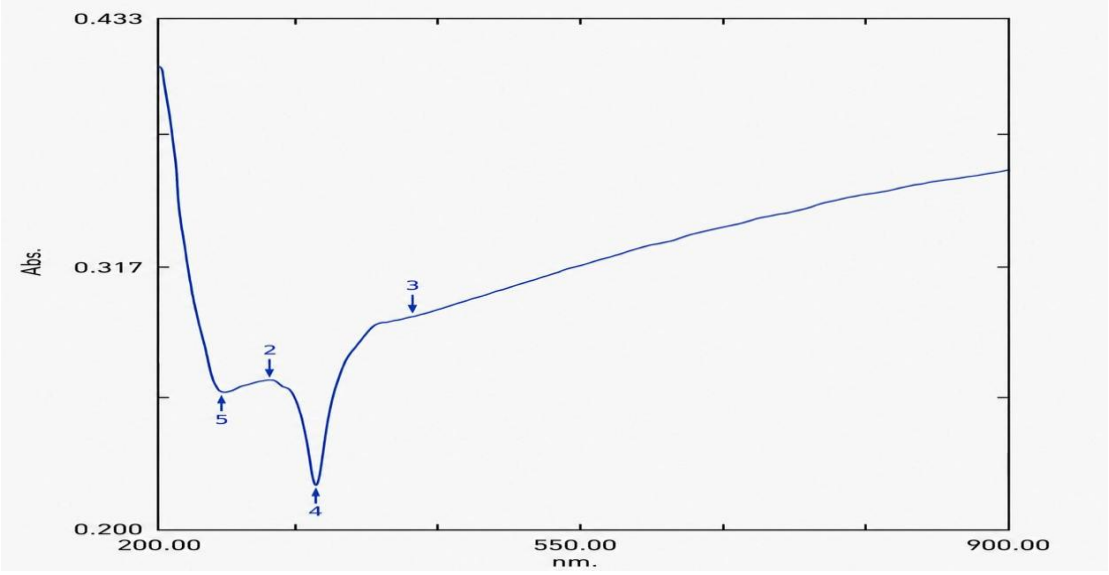

Fig. 1. UV–Vis Spectrophotometry absorption spectra recorded of AgNps peak was observed at 405 nm.

Statistical analysis

All measurements were performed in triplicate (n = 3) and results are reported as mean values. Descriptive statistics were calculated for each metric across all concentrations and time points. Comparative analysis between AgNps concentrations and iodine was performed to identify the optimal performance condition across all five metrics simultaneously**.**

RESULTS AND DISCUSSION

UV–Vis spectral analysis

AgNps were examined using UV–VIS spectrophotometry across a wavelength range of 100–1100 nm. The resulting spectrum, presented in Fig. 1, showed a well-defined surface plasmon resonance (SPR) absorption peak at 450 nm,. This observation falls within the characteristic UV–Vis absorption range reported for AgNps (400-500 nm), where the precise position of the SPR peak is known to shift depending on particle size, morphology, and the nature of the biological molecules coating the nanoparticle surface. Md Alim-Al-Razy et al. (2020)[16] and Mulu M et al. (2024)[17], both groups attributed the differences in peak position to variations in nanoparticle size and surface stabilization an interpretation that is consistent with the lower peak position observed here, which reflects the smaller particle size (25 nm) of the AgNps produced in this study. Beyond confirming the nanoparticles, the shape of the absorption peak itself carried important

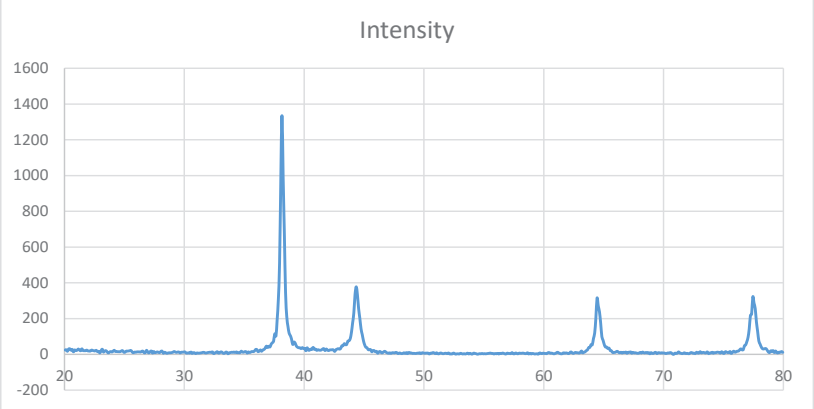

Fig. 2. XRD pattern of AgNPs.

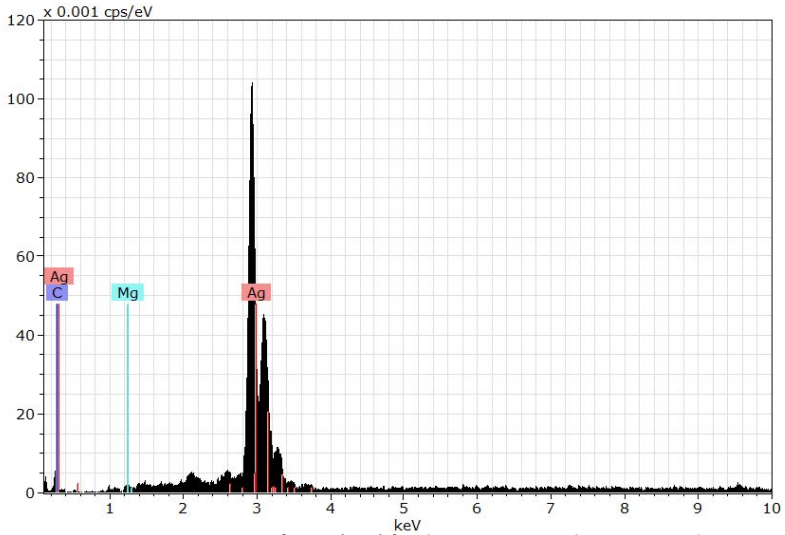

Fig. 3. Energy Dispersive of X-ray (EDS) for the Ag nanoparticles nanoparticle.

information about particle quality.

X-ray Diffraction (XRD)

The X-ray diffraction (XRD) pattern for silver nanoparticles AgNps powder is shown in (Fig. 2). The occurrence of the major peaks are aligned with the diffraction peaks of AgNps confirmed the crystal structures by Using standard protocols and applying Debye-Scherrer equation:

$$D=K\lambda/(\beta\cos\theta)$$

nanoparticle size was found to be approximately 22.7 nm.

EDS for AgNPs

To verify the AgNPs elemental, energy-dispersive X-ray spectroscopy (EDS) was performed, and the results are presented in (Fig. 3). The results showed strong silver signals(3 keV), along with weak oxygen and carbon peaks, which might have originated from the tuber extract. The results are consistent with previous studies that reported the strong peak for AgNPs at 3 keV [18,19]. The EDS quantitative analysis showedthe presence of silver (100%) without any contaminants.

Zeta potential (ZP) analysis

Zeta potential is referred to as being of primary indication of the internal stability of a colloid. It should be pointed out that AgNPs particles are referred to as being stable if they were either more negative than - 30 mV or more positive than +30 mV. It would be concluded that the AgNPs were very stable from (Fig. 4) displaying the zeta potential of AgNPs in the current study to be -11.28 mV which indicated that the suspension is electrostatically weakly stabilized and prone to aggregation under physiological or even ambient conditions. This finding is scientifically consistent with the time-dependent decline in X-ray contrast performance observed at the 5-minute time point in this study. This Zp-average is owed to the greater electrostatic repulsion between nanoparticles. The higher Zeta potential value indicates greater stability. In general, the zeta potential is an indication of the surface charges of NPs (negative or positive) and their magnitude [20].

The value of (−11.28 mV) is scientifically consistent with and directly explains several observations in this study:

Time-dependent contrast decline the drop in mean X-ray intensity between the 3-minute and 5-minute time points for most AgNPs concentrations is a direct physical consequence of this weak surface charge. With only −11.28 mV of electrostatic repulsion, Van der Waals attractive forces dominate progressively over time, driving particle aggregation and sedimentation within minutes. Concentration-dependent performance peak at 0.75 mg/kg at supra-optimal concentrations (1.0 mg/kg), the increased particle density brings weakly charged particles closer together in suspension, accelerating inter-particle collisions and aggregation. With a zeta potential of only −11.28 mV, there is insufficient electrostatic repulsion to counteract this crowding effect, which explains the paradoxical performance decline at higher concentrations.

Field Emission Scanning Electron Microscopy (FESEM) Of AgNPs

In SEM the sample of Ag NPs found the spherical shape and average size about (23-25.96) nm as

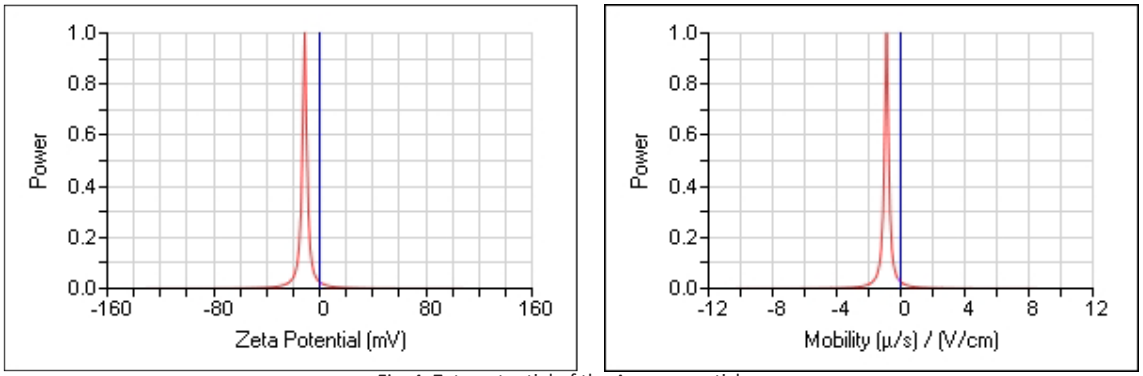

Fig. 4. Zeta potential of the Ag nanoparticles.

shown in Fig. 5.

Mean intensity

Mean intensity values are shown in Table 1.and Fig. 6. The highest mean intensity was observed in the AgNP 0.75 mg/kg group at 3 minutes after injection (84.56 arbitrary units). This value was higher than the iodine group at the same time point (30.76) and higher than the deionized water control (39.08). AgNPs at 0.50 mg/kg also

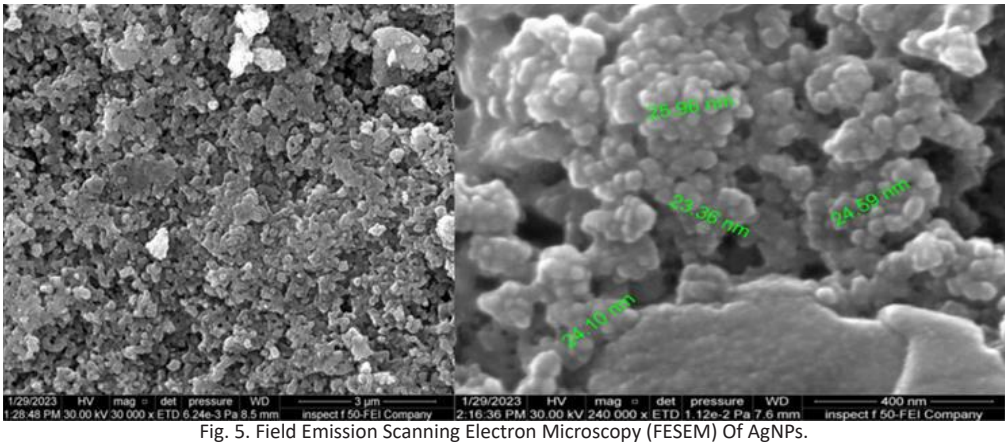

Fig. 5. Field Emission Scanning Electron Microscopy (FESEM) Of AgNPs.

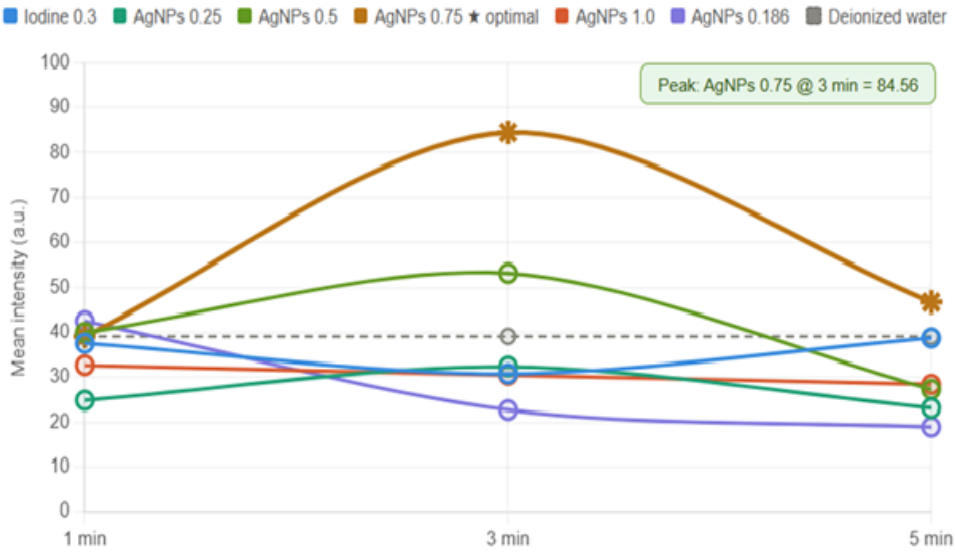

Fig. 6. Mean intensity values (arbitrary units) of all tested agents at three time points.

Table 1. Mean intensity values after intravenous injection.

Agent / reported dose	1 min	3 min	5 min
Iodine 0.30 mg/kg	37.53	30.76	38.72
AgNPs 0.25 mg/kg	24.81	32.35	23.11
AgNPs 0.50 mg/kg	39.96	53.16	27.26
AgNPs 0.75 mg/kg	39.06	84.56	46.69
AgNPs 1.00 g/kg	32.64	30.47	28.39
AgNPs 0.186 mg/kg	42.49	22.67	18.92
Deionized water	39.08	39.08	39.08

increased at 3 minutes (53.16), while the 0.25 mg/kg, 0.186 mg/kg, and 1.00 g/kg groups showed lower or less consistent values. These findings suggest that 0.75 mg/kg produced the strongest early X-ray signal in this dataset.

RMS contrast

RMS contrast values are summarized in Table 2 and Fig. 7. The AgNPs 0.186 mg/kg group showed high RMS contrast across all time points, and iodine showed a high RMS contrast at 3 minutes. However, RMS contrast mainly reflects pixel variability; it does not automatically prove superior contrast-agent performance. The AgNPs 0.75 mg/kg group showed high RMS contrast at 1 and 3 minutes, followed by a decrease at 5 minutes.

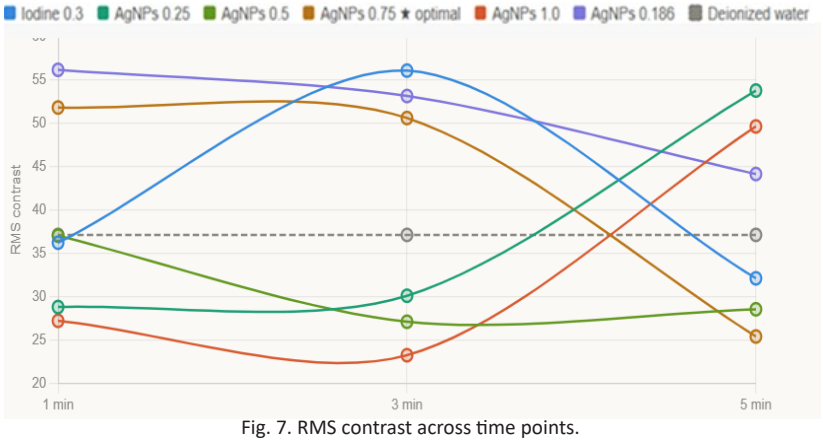

Fig. 7. RMS contrast across time points.

Table 2. RMS contrast values after intravenous injection.

Agent / reported dose	1 min	3 min	5 min
Iodine 0.30 mg/kg	36.22	56.07	32.11
AgNPs 0.25 mg/kg	28.80	30.10	53.77
AgNPs 0.50 mg/kg	37.03	27.10	28.54
AgNPs 0.75 mg/kg	51.81	50.60	25.40
AgNPs 1.00 g/kg	27.21	23.24	49.63
AgNPs 0.186 mg/kg	56.16	53.14	44.14
Deionized water	37.12	37.12	37.12

Table 3. Michelson contrast values after intravenous injection.

Agent / reported dose	1 min	3 min	5 min
Iodine 0.30 mg/kg	0.945	1.000	0.946
AgNPs 0.25 mg/kg	0.992	0.962	1.000
AgNPs 0.50 mg/kg	1.000	0.910	0.992
AgNPs 0.75 mg/kg	1.000	0.939	0.910
AgNPs 1.00 g/kg	0.961	0.946	0.992
AgNPs 0.186 mg/kg	1.000	1.000	1.000
Deionized water	0.969	0.969	0.969

Michelson contrast

Michelson contrast values are shown in Table 3 and Fig. 8. Most groups produced high values ranging from 0.910 to 1.000. Several groups reached the theoretical maximum of 1.000. However, the water control also produced a high value of 0.969, meaning that Michelson contrast was not highly discriminating in this imaging setup. Therefore, Michelson contrast should be treated as a supplementary metric rather than the main evidence of AgNPs superiority.

Entropy

Entropy values are shown in in Table 4 and Fig. 9. The highest entropy was recorded in the AgNPs 0.75 mg/kg group at 3 minutes (7.31). This was

Fig. 8. Michelson contrast by agent and time point.

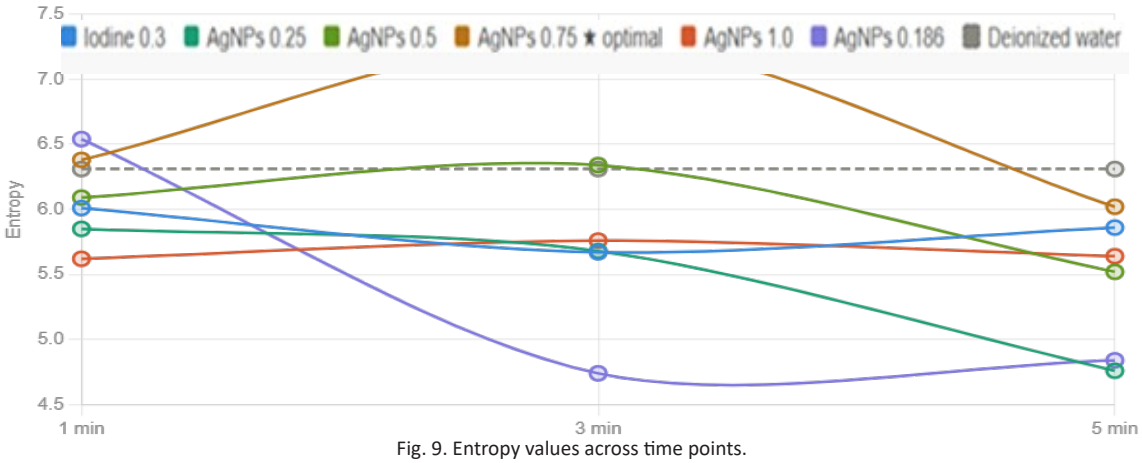

Fig. 9. Entropy values across time points.

Table 4. Entropy values after intravenous injection.

Agent / reported dose	1 min	3 min	5 min
Iodine 0.30 mg/kg	6.01	5.67	5.86
AgNPs 0.25 mg/kg	5.85	5.68	4.76
AgNPs 0.50 mg/kg	6.09	6.34	5.52
AgNPs 0.75 mg/kg	6.38	7.31	6.02
AgNPs 1.00 g/kg	5.62	5.76	5.64
AgNPs 0.186 mg/kg	6.54	4.74	4.84
Deionized water	6.31	6.31	6.31

higher than iodine at the same time point (5.67) and higher than deionized water (6.31). Because entropy reflects gray-level information content, this result suggests that AgNPs at 0.75 mg/kg produced the richest image information among the tested conditions. However, entropy can also be affected by noise, so future work should pair entropy with SNR and CNR.

Summary of optimal performance

A detailed table of height values is given in Table 5. AgNPs 0.75 mg/kg condition is the most convincing standard condition for 3 min because it blended the best adapted intensity with the best entropy. While other organizations have produced excessive RMS or Michelson contrast values, their metrics were much less specific and now need not be used by myself to provide the most complete contrast overall performance.

In a mouse tail-vein injection paradigm, this work offers an in vivo quantitative comparison of AgNPs and iodine as X-ray contrast agents. The primary conclusion is simple: AgNPs at 0.75 mg/kg generated the most pronounced overall improvement in image quality, particularly three minutes following injection. At that time, the dataset's mean intensity and entropy achieved their maximum values. This combination is significant because it shows richer gray-level information in the image in addition to a stronger signal. Physically and biologically, the outcome makes sense. Silver is appealing for low-energy and dual-energy X-ray imaging because of its K-edge, which is close to 25.5 keV. Silica-encapsulated silver nanoparticles have been created for dual-energy mammography applications, and prior research has suggested silver as a potential material for contrast-enhanced dual-energy breast imaging [4-6]. Although they should still be regarded as preliminary, the current results provide supporting in vivo image-quality data.The reaction was not just dose-dependent. The 0.75 mg/kg AgNP condition was not superior to the 1.00 g/kg AgNPs condition. This is not a mistake to conceal, but rather an essential remark. Better contrast is not necessarily correlated with higher doses. Nanoparticles may agglomerate, distribute less evenly, change local viscosity, or produce scattering and image saturation effects at very high concentrations. The precise cause cannot be determined without DLS, zeta potential, serum-stability testing, and biodistribution data. However, rather than a linear dose-response curve, the observed peak at 0.75 mg/kg shows that AgNP performance may have an ideal dose range. Additionally, the time profile is crucial. A number of indicators decreased by five minutes, but the best performance happened at three minutes. This could be the result of early redistribution, removal from the vascular compartment, reticuloendothelial system organ uptake, or blood particle instability. Size, coating, dose, administration method, and biological environment are known to have a significant impact on the toxicity and biodistribution of silver nanoparticles [7]. Thus, organ biodistribution, blood half-life, histopathology, and serum chemistry should be included in future imaging studies. It is important to properly analyze the Michelson contrast and RMS contrast results. Some groups that did not exhibit substantial mean intensity or entropy had considerable RMS contrast. This indicates that RMS contrast by itself may be deceptive since it gauges variability rather than providing a helpful diagnostic improvement. In a similar vein, even in the deionized water control, Michelson contrast was high. This suggests that rather than actual contrast-agent behavior, the metric may have been influenced by the image dynamic range or extreme pixels. This study's multi-metric methodology is one of its main advantages. The study employed numerical metrics that capture many aspects of image quality rather than depending solely on visual examination. Overall, the findings confirm AgNPs'

Table 5. Summary of peak image-quality values.

Agent / condition	Peak mean intensity	Peak RMS contrast	Peak entropy	Maximum Michelson contrast
Iodine 0.30 mg/kg	38.72 (5 min)	56.07 (3 min)	6.01 (1 min)	1.000 (3 min)
AgNPs 0.25 mg/kg	32.35 (3 min)	53.77 (5 min)	5.85 (1 min)	1.000 (5 min)
AgNPs 0.50 mg/kg	53.16 (3 min)	37.03 (1 min)	6.34 (3 min)	1.000 (1 min)
AgNPs 0.75 mg/kg	84.56 (3 min)	51.81 (1 min)	7.31 (3 min)	1.000 (1 min)
AgNPs 1.00 g/kg	32.64 (1 min)	49.63 (5 min)	5.76 (3 min)	0.992 (1 and 5 min)
AgNPs 0.186 mg/kg	42.49 (1 min)	56.16 (1 min)	6.54 (1 min)	1.000 (all)
Deionized water	39.08 (stable)	37.12 (stable)	6.31 (stable)	0.969 (stable)

potential as experimental X-ray contrast agents.

CONCLUSION

Silver nanoparticles (25nm) administered by lateral tail-vein injection showed promising in vivo X-ray contrast performance in mice. The most favorable condition was AgNPs at 0.75 mg/kg, particularly at 3 minutes after injection, where the highest mean intensity and entropy values were recorded. Iodine produced more moderate and relatively stable image-quality values. The 1.00 g/kg AgNPs condition did not improve performance, suggesting that AgNP contrast behavior may depend on an optimal dose range rather than a simple increase with dose. Future work should include complete animal-protocol reporting, calibrated attenuation values, SNR and CNR, nanoparticle physicochemical characterization, biodistribution, clearance, histology, and toxicity assessment before any clinical translation can be considered.

CONFLICT OF INTEREST

The authors declare that there is no conflict of interests regarding the publication of this manuscript.

REFERENCES

1. Davenport MS, Perazella MA, Yee J, Dillman JR, Fine D, McDonald RJ, et al. Use of Intravenous Iodinated Contrast Media in Patients with Kidney Disease: Consensus Statements from the American College of Radiology and the National Kidney Foundation. Radiology. 2020;294(3):660-668.
2. Hsu JC, Nieves LM, Betzer O, Sadan T, Noël PB, Popovtzer R, et al. Nanoparticle contrast agents for X-ray imaging applications. WIREs Nanomedicine and Nanobiotechnology. 2020;12(6).
3. Jiang Z, Zhang M, Li P, Wang Y, Fu Q. Nanomaterial-based CT contrast agents and their applications in image-guided therapy. Theranostics. 2023;13(2):483-509.
4. Karunamuni R, Maidment ADA. Search for novel contrast materials in dual-energy x-ray breast imaging using theoretical modeling of contrast-to-noise ratio. Phys Med Biol. 2014;59(15):4311-4324.
5. Karunamuni R, Tsourkas A, Maidment ADA. Exploring silver as a contrast agent for contrast-enhanced dual-energy X-ray breast imaging. The British Journal of Radiology. 2014;87(1041):20140081.
6. Karunamuni R, Naha PC, Lau KC, Al-Zaki A, Popov AV, Delikatny EJ, et al. Development of silica-encapsulated silver nanoparticles as contrast agents intended for dual-energy mammography. Eur Radiol. 2016;26(9):3301-3309.
7. Ferdous Z, Nemmar A. Health Impact of Silver Nanoparticles: A Review of the Biodistribution and Toxicity Following Various Routes of Exposure. Int J Mol Sci. 2020;21(7):2375.
8. Hsu JC, Lau KC, Barragan D, Mossburg KJ, Cormode DP, Maidment ADA. Influence of Acquisition Parameters on Silver Sulfide Nanoparticle Contrast in Photon-Counting Digital Mammography: A Phantom Study. ACS Applied Nano Materials. 2024;7(5):4805-4813.
9. Frequently Asked Questions About the Public Health Service Policy on Care and Use of Laboratory Animals: Prepared by the staff of the Division of Animal Welfare, Office for Protection from Research Risks, National Institutes of Health, Bethesda, Maryland. ILAR Journal. 1993;35(3-4):47-49.
10. Vines DC, Green DE, Kudo G, Keller H. Evaluation of Mouse Tail-Vein Injections Both Qualitatively and Quantitatively on Small-Animal PET Tail Scans. J Nucl Med Technol. 2011;39(4):264-270.
11. Rasmussen MK, Pedersen JN, Marie R. Size and surface charge characterization of nanoparticles with a salt gradient. Nature Communications. 2020;11(1).
12. Yuan T, Gao L, Zhan W, Dini D. Effect of Particle Size and Surface Charge on Nanoparticles Diffusion in the Brain White Matter. Pharm Res. 2022;39(4):767-781.
13. Nair V, Hoyt FH, Hoenen T, Fischer ER. Correlative Light and Electron Microscopy (CLEM) Techniques for Biological Samples. Microscopy and Microanalysis. 2013;19(S2):100-101.
14. Henry CR. Morphology of supported nanoparticles. Prog Surf Sci. 2005;80(3-4):92-116.
15. Holder CF, Schaak RE. Tutorial on Powder X-ray Diffraction for Characterizing Nanoscale Materials. ACS Nano. 2019;13(7):7359-7365.
16. Goodhew P. General Introduction to Transmission Electron Microscopy (TEM). Aberration-Corrected Analytical Transmission Electron Microscopy: Wiley; 2011. p. 1-19.
17. Ortiz Ortega E, Hosseinian H, Rosales López MJ, Rodríguez Vera A, Hosseini S. Characterization Techniques for Morphology Analysis. Progress in Optical Science and Photonics: Springer Singapore; 2022. p. 1-45.
18. Mazin k H. The Electron Microscopes: Concise History and Review. Iraqi Journal of Medical Sciences. 2022;20(2).
19. Parvesh D, Sushila S, Seema S, Promila D, Monika M. Effect of pH on Antioxidant and Phytochemical Activities of Mulhatti Roots (Glycyrrhiza glabra L.). Journal of Agricultural Science and Technology A. 2020;10(5).
20. Ramachandran T, Manoharan D, Natesan S, Rajaram SK, Karuppiah P, Shaik MR, et al. Synthesis and Structural Characterization of Selenium Nanoparticles–Bacillus sp. MKUST-01 Exopolysaccharide (SeNPs–EPS) Conjugate for Biomedical Applications. Biomedicines. 2023;11(9):2520.